

Wind line variability and intrinsic errors in observational mass loss rates

Derck Massa¹ and Raman Prinja²

¹Space Science Institute,
4750 Walnut Street Suite 205 Boulder, Colorado 80301, USA
email: dmassa@spacescience.org

²Department of Physics & Astronomy, University College London,
Gower Street, London WC1E 6BT, UK
email: rkp@star.ucl.ac.uk

Abstract. UV wind line variability in OB stars appears to be universal. We review the evidence that the variability is due to large, dense, optically thick structures rooted in or near the photosphere. Using repeated observations and a simple model we translate observed profile variations into optical depth variations and, consequently, variations in measured mass loss rates. Although global rates may be stable, measured rates vary. Consequently, profile variations infer how mass loss rates determined from UV wind lines vary. These variations quantify the intrinsic error inherent in any mass loss rate derived from a single observation. These derived rates can differ by factors of 3 or more. Our results also imply that rates from non-simultaneous observations (such as UV and ground based data) need not agree. Finally, we use our results to examine the nature of the structures responsible for the variability.

Keywords. stars: winds, outflows, stars: mass loss

1. Introduction

Wind line variability, as seen in H α , has been known for many years (e.g., Ebbets 1982). With the advent of *IUE*, it became clear that well developed but unsaturated UV wind lines in OB stars were also highly variable (e.g., Prinja & Howarth 1986). It is important to study this wind line variability for the following reasons: 1) It appears to be a universal property of radiatively driven winds. 2) Currently there are four ways to measure mass loss rates (\dot{M}): wind lines, IR/Radio excesses, X-rays and bow shocks. They do not all agree, due to structures (clumping) in the winds (e.g., Fullerton *et al.* 2006; Massa *et al.* 2017; Kobulnicky *et al.* 2019 AJ, 158, 73) and wind line variability *presents an opportunity to characterize these wind structures and provide feedback for modelers.* 3) Wind line variability *determines the intrinsic accuracy of a single measurement of \dot{M} .*

In the following, we discuss what is known about the nature and origin of the variability. We then introduce a simple model, use it to analyze the variability in a few times series and then summarize our results.

2. Observations of wind line variability

In this section we describe what has been learned from the morphology of wind line variability. Figure 1 shows examples of UV wind line variability in 4 stars with a range in spectral types, but all of which have well developed, but unsaturated Si IV λ 1400 resonance doublets. Figure 2 is the dynamic spectrum (a gray scale of all the spectra in a series divided by the mean) of a time series of the B0.5 Ib star, HD 64760, described by Massa *et al.* (1995). Such data sets have lead to the following conclusions.

Wind variability is universal: Wind line variability is seen in repeated observations of just about every OB star with a well developed but unsaturated wind line (e.g. Prinja & Howarth 1986). Further, it has also been observed in LMC and SMC OB stars (Massa *et al.* 2000) and the central stars of planetary nebulae (Prinja *et al.* 2012).

Spiral structures cause the variability: Time series of UV wind lines revealed bow shaped patterns in the dynamic spectra OB Stars (see Figure 2). Analysis of these patterns lead Cranmer & Owocki(1996) to interpret them in terms of co-rotating interaction regions (CIRs). However, any phenomenon that produces a spiral structure in the wind will do. To see the classic bow shape, one must view the star with $\sin i \simeq 1$ and the origin of the spot must be near the equator. Consequently, it is not surprising that the pattern is not seen in some stars with lower $v_{eq} \sin i$ s, although regularly repeating patterns are (Prinja *et al.* 2002).

The spiral structures are optically thick: Prinja & Massa (2010) applied a simple model to show that the Si IV $\lambda 1400$ doublet wind line profiles of a large sample of B supergiants are best fit using doublet ratios that are between unity and the actual ratio of the oscillator strengths of the doublet, $f_B/f_R \simeq 2$. This indicates that the line of sight to the stellar disk is partially covered by very optically thick structures, and by optically thin material. The result is a doublet absorption that appears unsaturated (because it does not go to zero) but whose relative strength is close to unity (since most of the absorption is from the strongly saturated optically thick component).

The spiral structures reach the stellar surface and are large: The fact that the variability appears to extend to $v \simeq 0$, does not necessarily mean that the physical structures extend to $r \simeq R_*$, since this could simply reflect a non-monotonic velocity law. However, Massa & Prinja (2015) showed that the absorption of the excited state line N IV 1718 blends smoothly with the high velocity absorption in resonance lines (see, Fig 3). Since N IV 1718 cannot exist without the strong photospheric radiation field, this analysis shows that the features must originate near $r = R_*$. Furthermore, since the features cause detectable absorption near R_* , they must occult a significant portion of the stellar disk.

The spiral structures are denser than ambient wind: A large change in the optical depth can indicate either a change in density, a flattening of the velocity law, or a change in the ionization (see, §3). It is, therefore, important to examine observational diagnostics that respond only to density. X-ray fluxes are one such diagnostic. It has been known for some time that the X-ray fluxes in OB stars are variable (see Oskinova *et al.* 2001, Nazé *et al.* 2013, Nazé *et al.* 2018). Most recently, Massa *et al.* (2019) obtained contemporaneous *XMM* X-ray and *HST* STIS UV spectra of the O7.5 III(n)((f)) star ξ Per. They were able to show that the X-rays are modulated by the spiral patterns, implying that they are significantly denser than the rest of the wind (the exact amount is model dependent).

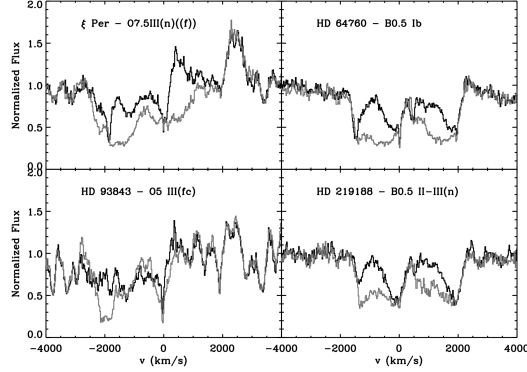


Figure 1. Examples of Si IV $\lambda\lambda 1400$ variability in four stars with a range in spectral types.

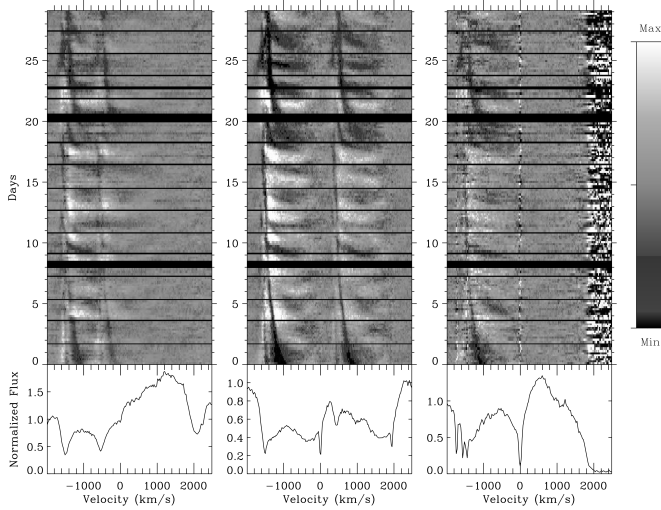


Figure 2. Dynamic spectra of (left to right) N V, Si IV and Si III for HD 64760 (B0.5 Ib, $v \sin i = 216 \text{ km s}^{-1}$. Massa *et al.* (1995).

3. Modeling wind line variability

In order to translate flux variations into the physical parameters needed to estimate the intrinsic error in a single \dot{M} measurement, a model is required. We use the SEI Sobolev model as formulated by Lamers *et al.* (1987) and modified by Massa *et al.* (2003).

The calculation of an SEI profile requires the following parameters:

- 1) A value for v_∞ (determined by a grid search),
- 2) A velocity law: typically a β -law, of the form $v = v_\infty(1 - a/x)^\beta$, where $x = r/R_\star$.

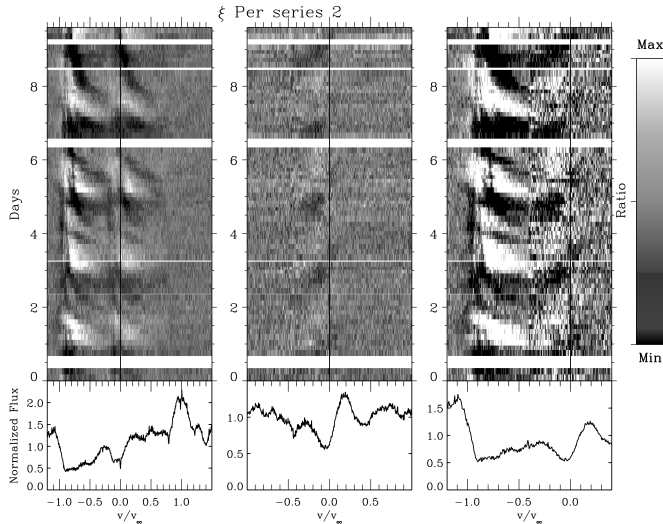


Figure 3. Dynamic spectra of Si IV, N IV, and the two spliced together for ξ Per ($v_\infty = 2450$ km s $^{-1}$, (Massa & Prinja 2015). Shows that structures are tied to the base of the wind where the radiation field is intense.

3) The radial (Sobolev) optical depth of the wind ($w = v/v_\infty$):

$$\tau_{rad}(w) = Const \frac{\dot{M}}{R_\star v_\infty^2} q_i(w) \left(x^2 w \frac{dw}{dx} \right)^{-1}$$

where $Const$ contains atomic parameters and q_i is the ionization fraction. $\tau_{rad}(w)$ is modeled by 20 velocity bins adjusted to obtain the best fitting profile. This approach can be viewed as an inversion of the profile to obtain $\tau_{rad}(w)$. *Note that τ_{rad} variations are proportional to derived $\dot{M}q$ variations.*

In addition to the usual parameters, we also allow the ratio of the optical depths of the doublets, f -ratio $\equiv f_B/f_R$, to vary. This is a well known means to mimic the effect of optically thick structures partially covering the stellar disk (Prinja & Massa 2015). It also provides an additional diagnostic of how the portion of the wind structures in front of the star varies with time. We also note that it has little affect on τ_{rad} . Its main effect is to improve the SEI fit to the red component of the wind line. All of these parameters are determined by a non-linear least squares fit to the observed profile.

4. Results

Figure 4 shows the quality of the fits that can be achieved. It shows non-linear least squares fits to the Si IV and N V profiles in ρ Leo. The model used $v_\infty = 1150$ km s $^{-1}$, and a TLUSTY (Lanz & Hubeny 2003) model with solar abundance and $(T_{eff}, \log g) = (25kK, 2.5)$ for the photospheric spectrum. The derived τ_{rad} s are shown below each spectrum, and the portion used to determine $\langle \tau \rangle$, $0.2 \leq v/v_\infty < 0.9$, is shaded gray. The best fit f -ratio and $\langle \tau \rangle$ values are also listed. Notice that the fit with the smaller $\langle \tau \rangle$ has the larger f -ratio.

As part of an ongoing program to analyze all repeated *IUE* observations of normal stars with well developed but unsaturated lines, we have begun with an analysis of a few time series. Figure 5 summarizes the results for two time series, one consisting of 70

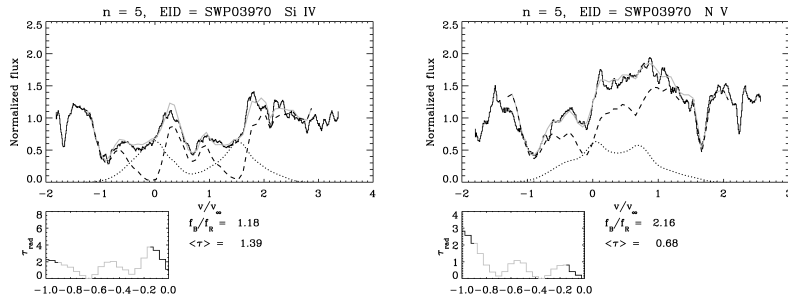


Figure 4. Fits to a Si IV and N V profiles in ρ Leo with derived τ_{rad} s below. Observed = solid black, fit = gray, absorbed photospheric profile = dashed and emission = dotted.

spectra of ξ Per and one for 146 spectra of HD 64760. The left hand panels show the mean τ_{rad} s and f -ratios versus time, while the right hand panels show the two quantities plotted against each other.

5. Analysis

The previous results can be used to address two distinct issues: the intrinsic error present in any \dot{M} derived from a single observation, and the nature of the structures responsible for the variations.

The intrinsic error: Recall that τ_{rad} is directly proportional to \dot{M} , so variations in τ_{rad} are a surrogate for variations in \dot{M} . Examination of the right panels of Figure 5 shows that the ranges of $\langle \tau_{rad} \rangle$ can be a factor of 3 or more. The means and variances of $\langle \tau_{rad} \rangle$ for the ξ Per series are = 1.09 and 0.27 and for the HD 64760 series they are 1.05 and 0.26. Both cases suggest the best accuracy one can expect is about $\pm 25\%$. However, this may be a lower limit since the distributions are highly non-Gaussian and the fact that the observations were clustered in time may introduce an additional bias. Nevertheless, a reasonable first estimate is $\sigma(\dot{M})/\dot{M} \simeq 1.25$, although this is probably a lower limit.

Constraints on the structures: It is interesting that, for the two series analyzed, the f -ratio varies periodically, as distinctly as the $\langle \tau_{rad} \rangle$ or even more so. Further, the f -ratio decreases as $\langle \tau_{rad} \rangle$ increases, suggesting that the change in the apparent optical depth is actually due to a larger fraction of the stellar surface being covered by optically thick material. These results are intriguing, but we emphasize that they are very preliminary.

6. Summary

We reviewed the evidence that wind line variability is universal and probably due to large, spatially coherent spiral structures. These structures extend to the base of the wind and cover much of the stellar disk. Further, they are denser than their surroundings, and because they are optically thick, *their geometry matters*. We then showed that the variability limits the intrinsic accuracy of a single \dot{M} measurement derived from a resonance line to roughly 25%, and that individual measurements can vary by as much as a factor of 3. This variability also compromises the consistency of non-simultaneous measurements. Finally, we discussed how our results can be used to constrain the nature of the structures responsible for the variability.

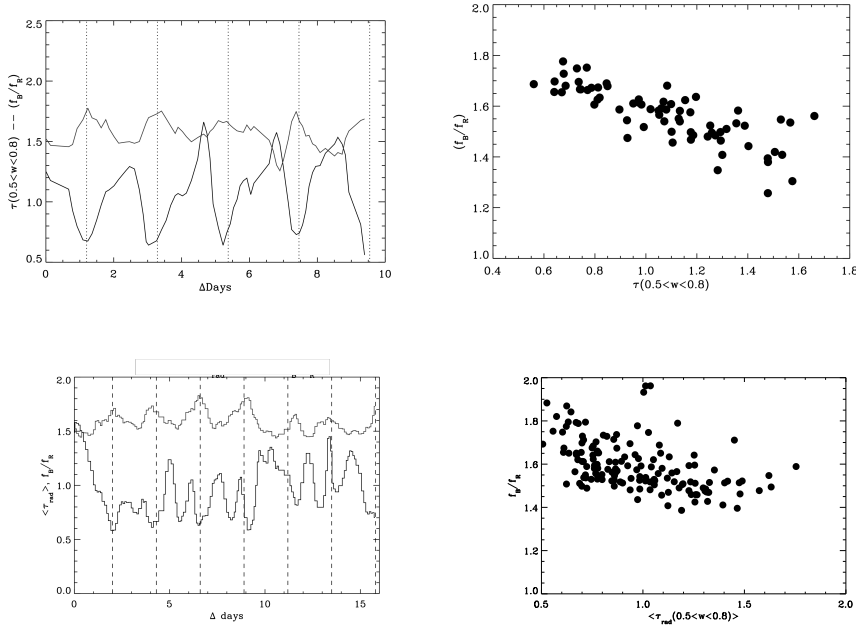


Figure 5. Top row: 70 Si IV spectra of ξ Per. Left: Variations of τ_{rad} averaged over $0.5 \leq v/v_\infty \leq 0.8$ (lower curve) and f -ratios (upper curve) versus days from first spectrum. Dotted vertical lines are the 2.086 day period determined by de Jong *et al.* (2001). Right: The same two quantities plotted against each other. **Bottom row:** 146 Si IV spectra of HD 64760. Left: Mean τ_{rad} s (lower curve) and f -ratios (upper curve) versus days from the first spectrum. Dotted vertical lines are a 2.30 Day period. Right: The same two quantities plotted against each other.

References

- Cranmer, S.R. & Owocki, S.P. 1996, *Ap.J.*, 462, 469
 Ebbets, D. 1982, *Ap.J. Supp.*, 48, 399
 de Jong, J.A., Henrichs, H.F., Kaper, L., *et al.* 2001, *A&A*, 368, 601
 Fullerton, A.W., Massa, D.L., & Prinja, R.K. 2006, *Ap.J.*, 637, 1025
 Lamers, H.J.G.L.M., Cerruti-Sola, M., & Perinotto, M. 1987, *Ap.J.*, 314, 726
 Lanz, T. & Hubeny, I. 2003, *Ap.J. Supp.*, 146, 417
 Massa, D., Fullerton, A.W., Nichols, J.S., *et al.* 1995, *Ap.J. Letters*, 452, L53
 Massa, D., Fullerton, A.W., Hutchings, J.B., *et al.* 2000, *ApJL*, 538, L47
 Massa, D. & Prinja, R.K. 2015, *ApJ*, 809, 12
 Massa, D., Oskinova, L., Prinja, R. & Ignace, R. 2019, *Ap.J.*, 873, 81
 Massa, D., Fullerton, A.W., Sonneborn, G., *et al.* 2003, *Ap.J.*, 586, 996
 Nazé, Y., Oskinova, L.M., & Gosset, E. 2013, *Ap.J.*, 763, 143
 Nazé, Y., Ramiaramanantsoa, T., Stevens, I.R., *et al.* 2018, *A&A*, 609, A81
 Oskinova, L.M., Clarke, D., & Pollock, A.M.T. 2001, *A&A*, 378, L21
 Fullerton, A.W., Massa, D.L., Prinja, R.K., *et al.* 1997, *A&A*, 327, 699
 Prinja, R.K. & Howarth, I.D. 1986, *Ap.J. Supp.*, 61, 357
 Prinja, R.K., Massa, D.L., Urbaneja, M.A., *et al.* 2012, *M.N.R.A.S.*, 422, 3142
 Prinja, R.K., Massa, D., & Fullerton, A.W. 2002, *A&A*, 388, 587
 Prinja, R.K. & Massa, D.L. 2010, *A&A*, 521, L55

Discussion